




The External Globus Pallidus as the Hub of the Auditory Cortico-Basal Ganglia Loop

 Ryohei Tomioka,^{1,2}  Naoki Shigematsu,³ Toshio Miyashita,^{4,5} Yukie Takahashi,³ Mariko Yamamoto,⁵ Yumiko Yoshimura,⁵ Kenta Kobayashi,⁶ Yuchio Yanagawa,⁷ Nobuaki Tamamaki,² Takaichi Fukuda,³ and  Wen-Jie Song^{1,8}

¹Department of Sensory and Cognitive Physiology, Faculty of Life Sciences, Kumamoto University, Kumamoto 860-8556, Japan, ²Morphological Neural Science, Graduate School of Life Sciences, Kumamoto University, Kumamoto 860-8556, Japan, and ³Department of Anatomy and Neurobiology, Faculty of Life Sciences, Kumamoto University, Kumamoto 860-8556, Japan, ⁴Department of Anatomy, Teikyo University School of Medicine, Tokyo 173-8605, Japan, ⁵Division of Visual Information Processing, National Institute for Physiological Sciences, Okazaki, Aichi 444-8585, Japan, ⁶Section of Viral Vector Development, National Institute for Physiological Sciences, Okazaki 444-8585, Japan, ⁷Department of Genetic and Behavioral Neuroscience, Gunma University Graduate School of Medicine, Maebashi 371-8511, Japan, and ⁸Center for Metabolic Regulation of Healthy Aging, Faculty of Life Sciences, Kumamoto University, Kumamoto 860-8556, Japan.

Abstract

The cortico-basal ganglia loop has traditionally been conceptualized as consisting of three distinct information networks: motor, limbic, and associative. However, this three-loop concept is insufficient to comprehensively explain the diverse functions of the cortico-basal ganglia system, as emerging evidence suggests its involvement in sensory processing, including the auditory systems. In the present study, we demonstrate the auditory cortico-basal ganglia loop by using transgenic mice and viral-assisted labelings. The caudal part of the external globus pallidus (GPe) emerged as a major output nucleus of the auditory cortico-basal ganglia loop with the cortico-striato-pallidal projections as its input pathway and pallido-cortical and pallido-thalamo-cortical projections as its output pathway. GABAergic neurons in the caudal GPe dominantly innervated the nonlemniscal auditory pathway. They also projected to various regions, including the substantia nigra pars lateralis, cuneiform nucleus, and periaqueductal gray. Considering the functions associated with these GPe-projecting regions, auditory cortico-basal ganglia circuits may play a pivotal role in eliciting defensive behaviors against acoustic stimuli.

Key words: auditory system; cortico-basal ganglia loop; globus pallidus; medial geniculate body; mouse

Significance Statement

The cortico-basal ganglia loops have been extensively studied. However, the auditory cortico-basal ganglia loop has remained elusive. In the present study, we demonstrated a cortico-basal ganglia loop in the auditory system. Our findings highlight GABAergic in the caudal external globus pallidus (GPe) as a major output nucleus in the auditory basal ganglia circuit. We identified principal targets of the caudal GPe, including the nonlemniscal auditory pathway, substantia nigra pars lateralis, cuneiform nucleus, and periaqueductal gray. Our findings provide novel insights into the auditory system and auditory-triggered behavior.

Introduction

The cortico-basal ganglia loop is known as a fundamental loop circuit in the forebrain. In the classical model of the basal ganglia, the striatum serves as the input nucleus, and the internal globus pallidus (GPi) and substantia nigra pars reticulata (SNR) function as the

Received April 12, 2024; revised Oct. 29, 2024; accepted Nov. 1, 2024.

The authors declare no competing financial interests.

Author contributions: R.T. designed research; R.T., N.S., T.M., Y.T., M.Y., K.K., and T.F. performed research; R.T., N.S., Y.T., and T.F. analyzed data; R.T., Yumiko Yoshimura, Yuchio Yanagawa, N.T., T.F., and W.-J.S. wrote the paper.

We thank the members of W.-J.S.'s laboratory for the discussion and Yuta Miyamoto (Kumamoto University) for the experimental advice. We also thank Yukiko Ikeda and Ryoko Mine at the Center for Metabolic Regulation of Healthy Aging, Faculty of Life Sciences, Kumamoto University, and the members of the Center for Animal Resources and Development, Kumamoto University for their technical

Continued on next page.

output nuclei via the various interconnected nuclei (Gerfen and Bolam, 2016). However, recent studies have revealed neuronal diversity within basal ganglia nuclei (Bolam et al., 2000; Mallet et al., 2012; Mastro et al., 2014; Abdi et al., 2015; Hernández et al., 2015; Oh et al., 2017; Abecassis et al., 2020; Ogata et al., 2022; Guilhemsang and Mallet, 2024). It has become evident that GABAergic neurons in the rostral external globus pallidus (GPe) represent a heterogeneous population, with distinct subgroups defined by their gene expression profiles and projection targets (Bolam et al., 2000; Mallet et al., 2012; Abdi et al., 2015; Oh et al., 2017; Abecassis et al., 2020). Notably, some GPe neurons project to the thalamus and cortex (Mastro et al., 2014; Saunders et al., 2015; Abecassis et al., 2020), suggesting that the GPe may serve as an output nucleus within the cortico-basal ganglia loop. This diversity in anatomical and neurochemical profiles suggests a more complex neural circuit than assumed in classical models.

Alexander et al. (1986) proposed five cortico-basal ganglia loops: motor, oculomotor, dorsolateral prefrontal, lateral orbitofrontal, and anterior cingulate gyrus. This model was later developed and conceptualized to process three types of information: motor, limbic, and associative (Joel and Weiner, 1994; Kompoliti and Metman, 2010; Simonyan, 2019). In this framework, the motor and oculomotor loops in Alexander's model are categorized as motor, the dorsolateral prefrontal and lateral orbitofrontal loops as associative, and the anterior cingulate loop as limbic. In the context of cortico-basal ganglia loops for sensory inputs, Alexander et al. (1986) documented somatosensory inputs within the framework of the motor loop, while Middleton and Strick (1996) demonstrated a cortico-basal ganglia loop associated with higher-order visual areas in primates, involving the cortico-striato-nigro-thalamo-cortical loop circuit, using herpes simplex virus Type 1. Despite these findings, descriptions of cortico-basal ganglia loops for sensory modalities remain limited, with no detailed descriptions related to auditory processing. Interestingly, some researchers have proposed roles of the basal ganglia in auditory and visual processing (Seger, 2013; Lim et al., 2014). In addition, recent systematic anatomical analyses have revealed that almost all cortical areas (including the auditory cortex) send excitatory projections to the striatum (Hintiryan et al., 2016; Hunnicutt et al., 2016; Miyamoto et al., 2018; Foster et al., 2021), suggesting that the cortico-basal ganglia loop is involved in a more diverse range of brain functions than previously concepts for motor, limbic, and associative processes.

Several lines of evidence suggest the presence of a cortico-basal ganglia loop associated with the auditory system. First, in both rodents and humans, the auditory cortex projects to the extreme caudal region of the striatum, known as the tail of the striatum (TS; Oh et al., 2014; Hintiryan et al., 2016; Hunnicutt et al., 2016; Miyamoto et al., 2018; Valjent and Gangarossa, 2021; Sitek et al., 2023). Additionally, recent systematic investigations have revealed that neurons in the TS project to the caudal GPe (Foster et al., 2021; Valjent and Gangarossa, 2021). These anatomical findings suggest that the caudal striato-pallidal pathway constitutes a part of the auditory cortico-basal ganglia loop. Second, recent physiological studies have demonstrated the roles of the corticostriatal pathway in the auditory cortex (Znamenskiy and Zador, 2013; Zhong et al., 2014; Xiong et al., 2015; Ponvert and Jaramillo, 2019; Li et al., 2021). However, the presence of the auditory cortico-basal ganglia loop remains elusive.

In this study, we utilized a variety of anatomical techniques to delineate the cortico-basal ganglia loop in the auditory system. Our findings not only reveal the neuronal circuits in this loop but also elucidate its connections to other brain regions. This intricate connectivity provides insight into how auditory information is processed in the brain. Overall, our study contributes to the anatomical understanding of the cortico-basal ganglia loop in the auditory system.

Materials and Methods

All surgical procedures were performed in accordance with the National Institutes of Health (NIH) "Guidelines for the Care and Use of Laboratory Animals" (NIH publication 86-23), and all protocols were approved by the Kumamoto University Animal Experiment Committee and the Experimental Animal Committee of the National Institute for Physiological Sciences. All efforts were made to minimize animal suffering and to reduce the number of animals used.

The animals (23–30 g at the time of injection) were housed in a ventilated room under standard conditions, including an air-conditioned environment at 20–25°C and 40–60%

support.

This work was supported by Japan Society for the Promotion of Science KAKENHI Grant Number 21K06442 (R.T.), 19K06908, 22K06433, 19H05222 (W.-J.S.), and 15H01443 (N.T.) and by Cooperative Study Program (22NIPS129 and 23NIPS124) of National Institute for Physiological Sciences.

Correspondence should be addressed to Ryohei Tomioka at tomioka@kumamoto-u.ac.jp.

Copyright © 2024 Tomioka et al. This is an open-access article distributed under the terms of the Creative Commons Attribution 4.0 International license, which permits unrestricted use, distribution and reproduction in any medium provided that the original work is properly attributed.

humidity, with a 12 h light/dark cycle. Adult male C57BL/6J mice ($n = 9$; SLC, Hamamatsu), glutamate decarboxylase 67 (GAD67)-Cre knock-in mice ($n = 16$; bred in the animal facility of Kumamoto University; Higo et al., 2009; Tomioka et al., 2015), GAD67-green fluorescent protein (GFP) knock-in mice ($n = 14$; bred in the animal facility of Kumamoto University; Tamamaki et al., 2003), and vesicular GABA transporter (VGAT)-Cre knock-in mice (RRID: IMSR_JAX:028862) that were back-crossed with the C57BL/6J strain ($n = 12$; bred in the animal facility of National Institute for Physiological Sciences) were used in this study.

Production of EnvA pseudotyped rabies virus expressing mCherry. The pseudotyped rabies virus, EnvA-HEP- Δ G-mCherry, was used to label presynaptic neurons. EnvA-HEP- Δ G-mCherry was produced as previously described protocols (Osakada et al., 2011; Mori and Morimoto, 2014). Briefly, to produce glycoprotein-deleted rabies virus HEP strain (HEP- Δ G-mCherry), the plasmid containing mCherry and the entire rabies virus genome without rabies glycoprotein and each plasmid containing rabies nucleoprotein, phosphoprotein, and polymerase genes were transfected to BHT-T7/9 cells (TransIT-LT1; Takara Bio). The cell culture plates were incubated for 2–4 d at 32°C in an atmosphere containing 5% CO₂. Once the number of mCherry-positive cells increased, the culture supernatant was collected and transferred to BHK-SiG cells, which express SADcvsG glycoproteins, to raise the virus titer of HEP- Δ G-mCherry virus. The cell culture medium containing HEP- Δ G-mCherry virus was collected and transferred to BHK-Lv-EiG cells, which express avian sarcoma leucosis virus envelope protein (EnvA), to produce pseudotyped rabies virus, EnvA-HEP- Δ G-mCherry. The cell culture plates were incubated for 4–5 d at 32°C in an atmosphere containing 3% CO₂. EnvA-HEP- Δ G-mCherry virus was collected from the cell culture medium by centrifugation. The contamination of unpseudotyped rabies virus HEP- Δ G-mCherry in the concentrated virus was examined using HEK293T. Infection of unpseudotyped rabies virus was not confirmed in vitro. We confirmed an infectious titer of EnvA-HEP- Δ G-mCherry virus in 293-TVA cells.

Surgical procedures and fixation. Each animal was deeply anesthetized with a mixture of ketamine (80 mg/kg, i.p.; Fujita) and xylazine (8 mg/kg; Elanco) and placed in a stereotaxic frame (Narishige). A craniotomy was performed at the appropriate skull location. All injections were performed by air pressure using a custom-made syringe pump connected to a glass capillary needle (Calibrated micropipettes 2-000-001, Drummond Scientific). For the anterograde transneuronal tracing experiment, we injected 0.2 μ l of adeno-associated virus [AAV; AAV1-CMV-HI-eGFP-Cre: 2.8×10^{12} viral genomes per μ l (vg/ml), Addgene Viral Prep#105545-AAV1; Addgene] into the primary auditory cortex (A1; bregma, –3.0 mm; lateral, 4.5 mm; depth, 0.5 mm) and 0.1 μ l of AAV2-CAG-FLEX-tdTomato (1.2×10^{13} vg/ml, University of North Carolina Vector Core) into the TS (bregma, –1.3 mm; lateral, 3.6 mm; depth, 2.7 mm). The survival time for the anterograde transneuronal tracing experiment was 3 weeks. To visualize axonal fibers from GPe GABAergic neurons, we injected 0.08 μ l of AAV2-CAG-FLEX-GFP (2.2×10^{13} vg/ml, University of North Carolina Vector Core) into the GPe of GAD67-Cre mice (bregma, –1.2 mm; lateral, 2.7 mm; depth, 3.2 mm). The survival time for the anterograde experiment was 3 weeks. We injected 0.02 μ l of Fluoro-Gold (FG; 4% dissolved in water; Fluorochrome) into GAD67-GFP mice as a retrograde tracer. The FG-injection sites are the temporal association cortex (bregma, –3.0 mm; depth, 0.5 mm from the cortical surface at a 50° angle from the horizontal plane), medial geniculate body (MGB; bregma, –3.0 mm; lateral, 2.0 mm; depth, 3.0 mm), and cuneiform nucleus (CnF; bregma, –5.0 mm; lateral, 1.5 mm; depth, 2.0 mm). The survival time for the retrograde experiments was 3 d. To identify the presynaptic neurons of GPe GABAergic neurons, we injected 0.2 μ l of a virus mixture (AAVretro-CA-FLEX-SADcvsG, 2.0×10^{12} vg/ml, and AAVretro-EF1a-FLEX-GFP-2A-TVA, 9.8×10^{11} vg/ml in National Institute for Physiological Sciences, Section of Viral Vector Development) into the temporal association cortex of VGAT-Cre mice (bregma, –3.0 mm; depth, 0.5 mm from the cortical surface at a 50° angle from the horizontal plane). Three weeks later, 0.2 μ l of pseudotyped rabies virus (EnvA-HEP- Δ G-mCherry, 2.3×10^8 infectious units/ml) was injected into the caudal GPe (bregma, –1.2 mm; lateral, 2.7 mm; depth, 3.2 mm). The survival time after the second injection was 7 d. We performed two control experiments using pseudotyped rabies virus. To confirm the contamination of unpseudotyped rabies virus in vivo, AAVretro-CA-FLEX-SADcvsG and AAVretro-EF1a-FLEX-GFP-2A-TVA were injected into A1 of C57BL/6J mice, following the injection of pseudotyped rabies virus into the same area. In another control experiment, to confirm the distribution of starter cells, AAVretro-EF1a-FLEX-GFP-2A-TVA were injected into the temporal association cortex of VGAT-Cre mice, following the injection of pseudotyped rabies virus into the caudal GPe.

For confocal microscopic examination, mice were perfused with 0.05 M phosphate-buffered saline [PBS; 0.9% (w/v) saline buffered with 0.05 M sodium phosphate], pH 7.4, followed by 4% formaldehyde in PBS under deep anesthesia (ketamine, 120 mg/kg; xylazine, 12 mg/kg). The brains were cryoprotected with 30% sucrose in PBS, and 50- μ m-thick coronal sections were cut using a cryostat (CM1950, Leica Biosystems). For electron microscopic examination, mice were deeply anesthetized and then perfused with PBS, pH 7.4, followed by 50 ml of a mixture of 0.1% glutaraldehyde and 4% paraformaldehyde in 0.1 M PB at room temperature. Brains were removed from the skull and stored overnight in 4% paraformaldehyde in 0.1 M PB at 4°C. The fixative was replaced by PBS. Serial 40- μ m-thick coronal sections were cut using a vibrating microtome (model TTK-3000, Dosaka). Histological analysis was conducted according to the mouse brain atlas to identify specific brain structures (Franklin and Paxinos, 2007).

Fluorescent immunostaining. To identify the anatomical or neurochemical properties, we performed immunostaining using the following primary antibodies (see the detailed information in Table 1): a mouse anti-calretinin (CR) antibody (Swant), goat anti-choline acetyltransferase (ChAT) antibody (Merck), rabbit anti-FG antibody (Merck), goat anti-forkhead box protein P2 (FoxP2) antibody (Santa Cruz Biotechnology), rabbit anti-GFP antibody (Tomioka et al., 2015), mouse anti-LIM Homeobox 6 (Lhx6) antibody (Santa Cruz Biotechnology), rabbit anti-NeuN antibody (Abcam), guinea pig anti-parvalbumin (PV) antibody (NITTOBO MEDICAL), mouse anti-PV antibody (Swant), mouse anti-protein kinase C δ (PKC δ) antibody (BD Transduction Laboratories), rabbit anti-prodynorphin (PD) antibody (Abcam), rabbit anti-preproenkephalin (PPE) antibody (Neuromics), rabbit anti-synaptophysin antibody (NITTOBO MEDICAL), and mouse anti-tyrosine hydroxylase (TH) antibody (Santa Cruz Biotechnology). After blocking with PBS containing 0.3% Triton X-100 and 1% normal donkey serum for 1 h at room temperature, sections from at least three animals were incubated with primary antibodies overnight at room temperature in a blocking solution. The sections were incubated with an appropriate set of secondary antibodies labeled with fluorescent dyes at different wavelengths for 2 h at room temperature (Table 2). Images were obtained using a confocal laser scanning microscope (FV3000; Olympus) with appropriate filters for Alexa Fluor 488 (laser wavelength, 488 nm; detection wavelength, 500–540 nm), Alexa Fluor 555 (laser wavelength, 561 nm; detection wavelength, 570–620 nm), or Alexa Fluor 647 (laser wavelength, 640 nm; detection wavelength, 650–750 nm). Images were merged using Canvas 12 (Canvas GFX), and some were displayed in a pseudocolor format.

Correlated confocal laser scanning light microscopy (CLSM)–electron microscopy (EM). Five mice were used for CLSM–EM examination. The CLSM–EM method was performed as described previously with slight modifications (Fukuda, 2017; Shigematsu et al., 2019; Ogata et al., 2022). After cryoprotection with 25% sucrose in PBS, the sections placed on aluminum foil were quickly frozen in liquid nitrogen vapor and rapidly thawed with 25% sucrose in PBS. The sections were incubated with 1% bovine serum albumin (Merck) and 0.1% sodium azide in PBS for 1 h, followed by

Table 1. List of primary antibodies used in this study

Primary antibody	Dilution	Host species
CR (Swant, 6B3)	1:1,000	Mouse
CR (Swant, 7699/4)	1:5,000	Rabbit
ChAT (Merck, AB144P)	1:1,000	Goat
FG (Merck, AB153-l)	1:2,000	Rabbit
FoxP2 (Santa Cruz Biotechnology, sc-21069)	1:1,000	Goat
GFP (Nacalai, GF200)	1:1,000	Rat
GFP (Tomioka et al., 2015)	1 μ g/ml	Rabbit
Lhx6 (Santa Cruz Biotechnology, sc-271433)	1:100	Mouse
NeuN (Abcam, ab177487)	1:1,000	Rabbit
PV (NITTOBO MEDICAL, MSFR105250)	1:200	Guinea pig
PV (Swant, 235)	1:500	Mouse
PKC δ (BD Transduction Laboratories, 610398)	1:500	Mouse
PD (Abcam, ab11137)	1:100	Rabbit
PPE (Neuromics, RA14124)	1:8,000	Rabbit
Synaptophysin (NITTOBO MEDICAL, MSFR105660)	1:200	Rabbit
Tyrosine hydroxylase (Santa Cruz Biotechnology, sc-25269)	1:500	Mouse

Table 2. List of secondary antibodies used in this study

Second antibody	Dilution	source	Catalog#
Alexa Fluor 488-conjugated donkey anti-mouse IgG	1:1,000	Thermo Fisher Scientific	A-32766
Alexa Fluor 488-conjugated donkey anti-rabbit IgG	1:1,000	Thermo Fisher Scientific	A-32790
Alexa Fluor 555-conjugated donkey anti-mouse IgG	1:1,000	Thermo Fisher Scientific	A-31570
Alexa Fluor 555-conjugated streptavidin	1:1,000	Thermo Fisher Scientific	S-21381
Alexa Fluor 647-conjugated donkey anti-mouse IgG	1:1,000	Thermo Fisher Scientific	A-32787
Alexa Fluor 647-conjugated donkey anti-guinea pig IgG	1:1,000	Thermo Fisher Scientific	A-21450
Alexa Fluor 647-conjugated donkey anti-rabbit IgG	1:1,000	Thermo Fisher Scientific	A-32795
Alexa Fluor 647-conjugated streptavidin	1:500	Jackson ImmunoResearch Laboratories	016-600-084
Biotiny-SP-conjugated donkey anti-rat IgG	1:250	Jackson ImmunoResearch Laboratories	712-065-153
Biotiny-SP-conjugated donkey anti-goat IgG	1:1,000	Thermo Fisher Scientific	A-16009
Biotiny-SP-conjugated goat anti-guinea pig IgG	1:1,000	Thermo Fisher Scientific	A-18779
Peroxidase anti-peroxidase	1:500	Jackson ImmunoResearch Laboratories	323-005-024
Rhodamine red-conjugated donkey anti-rabbit IgG	1:200	Jackson ImmunoResearch Laboratories	711-295-152

incubation with a mixture of primary antibodies containing rabbit anti-CR (1:5,000; Swant) antibody and rat anti-GFP (1:500; Nacalai) at 4°C for 4 d. After rinsing several times in PBS, the sections were incubated with biotinylated anti-rat IgG (1:250; Jackson ImmunoResearch Laboratories) at 4°C overnight, followed by incubation with Alexa Fluor 647-conjugated streptavidin (Molecular Probes) and Rhodamine Red-conjugated anti-rabbit IgG (1:200; Jackson ImmunoResearch Laboratories) at 4°C overnight.

Appositions of GFP-positive boutons on CR-positive neurons were examined using a 40× objective lens. After CLSM, coverslips were removed, and the sections were treated with the ABC method (Vector Laboratories) using the DAB-Ni peroxidase reaction to visualize GFP-positive axonal fibers. After the reaction, the sections were rinsed overnight in PBS containing 0.1% sodium azide at 4°C. After several rinses in PBS, the sections were incubated with rabbit peroxidase anti-peroxidase complex (Jackson ImmunoResearch Laboratories, 1:500) in PBS at 4°C overnight. After several rinses in PBS, sections were treated with a DAB-peroxidase reaction, followed by OsO₄ postfixation, en bloc staining with 1.5% uranyl acetate, dehydration in ethanol, and embedding in Epon-Araldite. Synaptic connections between GFP-positive boutons and CR-positive neurons at the apposition sites observed by CLSM were examined by EM (HT7700, Hitachi).

Image data analysis. Five mice were used for the quantitative measurements of axonal fibers. Image analysis was performed using a previously described method, with slight modifications (Tomioka et al., 2023). Similar coronal sections were analyzed for the quantitative measurement of GFP-labeled axonal fibers from the GPe. Images were obtained using a confocal laser scanning microscope (FV3000) with a 10× objective lens at a 2,048 × 2,048 pixel resolution. All images were analyzed using the MATLAB software (R2019b; MathWorks). Briefly, the boundaries of the MGB subdivisions were defined according to PKCδ immunoreactivity (Tomioka et al., 2023). The area of each subdivision was calculated. The raw images of GFP-positive signals were converted into binary images using one threshold per section. The summed area of GFP-positive signals in each subdivision was calculated. Finally, the occupancy of GFP-positive signals in each MGB subdivision was computed. Friedman's test and Bonferroni's post hoc test were used for multiple comparisons.

Six mice were used for quantitative measurement of Lhx6 immunoreactivity. Images were obtained using a confocal laser scanning microscope (FV3000) with a 40× objective lens at a 2,048 × 2,048 pixel resolution. We measured the intensity of Lhx6 immunoreactivity in the caudal GPe. We calculated the average intensities of Lhx6 immunoreactivity in PV-positive and PV-negative neurons in each animal. A two-tailed paired *t* test was used for statistical analysis. Statistical significance was set at *p* < 0.05.

Results

Auditory striatal projecting neurons

Recent systematic studies utilizing large tracing datasets have provided detailed maps of corticostriatal and striato-pallidal projections, suggesting the existence of a neural network for auditory information processing in the basal ganglia (Hintiryan et al., 2016; Hunnicutt et al., 2016; Foster et al., 2021; Valjent and Gangarossa, 2021; Ogata et al., 2022). First, we examined auditory-related striatal projections using anterograde transneuronal tracing. Because AAV serotype 1 allows for anterograde transneuronal labeling (Zingg et al., 2017), Cre recombinase was introduced into striatal neurons by injecting AAV1-CMV-HI-eGFP-Cre into A1 (Fig. 1A). With an additional injection of AAV2-CAG-FLEX-tdTomato into the TS, postsynaptic striatal neurons were labeled with tdTomato in a Cre-dependent manner (Fig. 1B). The distribution of tdTomato-labeled axonal fibers was predominantly observed in the caudal GPe (Fig. 1C,D), followed by the substantia nigra pars lateralis (SNL; Fig. 1E; Extended Data Fig. 1-1), but did not extend to the GPi and SNR (data not shown). Since the GPe would be on the major pathway of the auditory cortico-basal ganglia loops, we extensively analyzed the neural circuit via the caudal GPe (−1.06 to −1.7 mm from the bregma along the rostrocaudal axis) in the present study.

Anterograde tracing from GABAergic neurons in the caudal GPe

We demonstrated that the caudal GPe is involved in the auditory cortico-basal ganglia loop. In addition, accumulating neuroanatomical and physiological evidence indicates that the caudal GPe is related to auditory function (Moriizumi and Hattori, 1992; Shammah-Lagnado et al., 1996; Zhong et al., 2014; Chavez and Zaborszky, 2017; Foster et al., 2021). We next examined the axonal projections from GABAergic neurons in the caudal GPe. AAV2-CAG-FLEX-GFP was injected into the caudal GPe of the GAD67-Cre mice. The injection sites were localized within the GPe in five mice, as illustrated and further analyzed (Fig. 2A). The GFP-immunoreactive axonal fibers were found mainly in and around the MGB (Fig. 2B), moderately in the CnF (Fig. 2D), and sparsely in the periaqueductal gray (PAG; Fig. 2D), temporal association area (TeA), and ectothalamic cortex (Ect; Fig. 2C). Pallido-cortical fibers were widely distributed across the rostral–caudal axis of the TeA/Ect. Our anatomical evidence aligns with the previous study using anterograde and retrograde tracing (Shammah-Lagnado et al., 1996), which demonstrated that GPe GABAergic neurons project to the lateral hypothalamus and substantia nigra pars lateralis. Thus, the present study is the first to demonstrate that GPe GABAergic neurons also project to the CnF and cortical areas.

We further analyzed the densities of GFP-immunoreactive axonal fibers in four subdivisions of the MGB according to anatomical and neurochemical properties (Llano and Sherman, 2008; Márquez-Legorreta et al., 2016; Tomioka et al., 2023). These subdivisions include the ventral division of the MGB (MGv), dorsal division of the MGB (MGd), medial and internal division of the MGB (MGm/MGi; Tomioka et al., 2023), and posterior intralaminar nucleus and peripeduncular

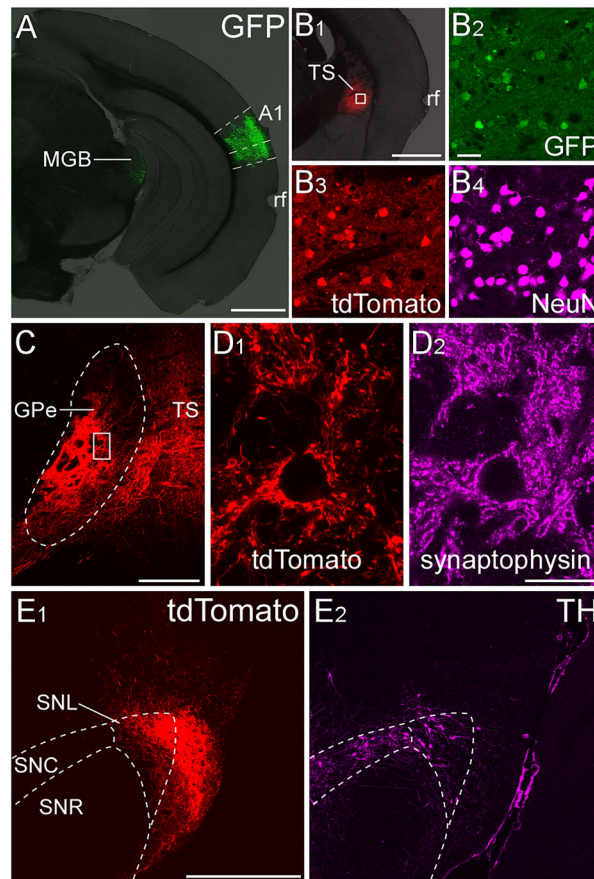


Figure 1. Axonal fibers of striatal neurons receiving auditory corticostriatal projections. **A**, AAV1-CMV-HI-eGFP-Cre was injected into A1. The injection site was mainly confined in the A1. The rhinal fissure (rf) is shown as a brain region marker. **B₁**, AAV2-CAG-FLEX-tdTomato was injected into the TS. **B₂–B₄**, The enlarged image of the area marked by the rectangle of **B₁**. The tdTomato-expressing neurons were found within the TS. **C**, Dense tdTomato-positive striatal fibers were in the caudal GPe. **D₁**, The enlarged image of the area marked by the rectangle of **C**. The distribution of tdTomato-positive axon terminals was similar to that of synaptophysin immunoreactivity in the caudal GPe (**D₂**). **E₁**, tdTomato-positive striatal fibers were in the SNL, but not in the SNC or reticulata (SNR). **E₂**, TH-immunoreactivity was used to define the boundaries of the substantia nigra. See Extended Data Figure 1-1 for more details. Scale bars: 1.0 mm in **A** and **B₁**, 50 μ m in **B₂**, 250 μ m in **C**, 25 μ m in **D**, and 500 μ m in **E**.

nucleus (PIN/PP). The PKC δ immunoreactivity exhibited distinct boundaries of MGB subnuclei, with uniform PKC δ immunoreactivity in MGv, gradient PKC δ immunoreactivity in MGd, and poor PKC δ immunoreactivity in MGm/MGi and PIN/PP (Fig. 3B). The distribution of GFP-immunoreactive axonal fibers was primarily in the MGd and MGm/MGi, secondary in the PIN/PP, and rarely in the MGv (Fig. 3A,C). Considering that the MGv is on the lemniscal pathway of the central auditory system while the others are on nonlemniscal pathways, our findings suggest that GABAergic neurons in the caudal GPe exert an inhibitory effect on the nonlemniscal auditory pathway.

The distribution pattern of GFP-immunoreactive axonal fibers in and around the MGB was similar to that of CR-expressing neurons (Llano and Sherman, 2008; Márquez-Legorreta et al., 2016; Tomioka et al., 2023). Of note, several studies have reported CR-expressing neurons in both the MGd and PIN/PP project to the temporal cortices including TeA/Ect and ventral part of the secondary auditory cortex (AuV) and lateral amygdala (Cai et al., 2019; Barsy et al., 2020; Belén Pardi et al., 2020). We next examined whether GABAergic neurons in the caudal GPe form synaptic contacts with CR-immunoreactive neurons. The CR-immunoreactive neurons were mainly distributed in the MGd and PIN/PP (Fig. 4-1), which is consistent with previous reports (Lu et al., 2009). Under CLSM observation, GFP-immunoreactive puncta of GPe GABAergic projection neurons were found in close apposition with the CR-immunoreactive somata in the PIN/PP and MGd (Fig. 4; Extended Data Fig. 4-2, respectively). To assess potential synaptic connections by CLSM, we performed double-labeled immunoelectron microscopy. CR and GFP immunoreactivities were visualized DAB and DAB-nickel as chromogenic agents, respectively (Fig. 4). The GFP-positive axon terminals forming symmetrical synapses on the CR-immunoreactive soma were observed in the PIN/PP (Fig. 4) and MGd (Extended Data Fig. 4-2) at the EM level. This finding suggests that GABAergic neurons in the caudal GPe may exert an inhibitory modulation on the temporal cortices and lateral amygdala by regulating the activity of CR-expressing neurons in the MGd and PIN/PP. Since GABAergic neurons in the caudal GPe directly project to the temporal cortices (Fig. 2C), they may suppress the temporal cortices via two pathways: the direct pallido-cortical pathway and the indirect pallido-thalamo-cortical pathway.

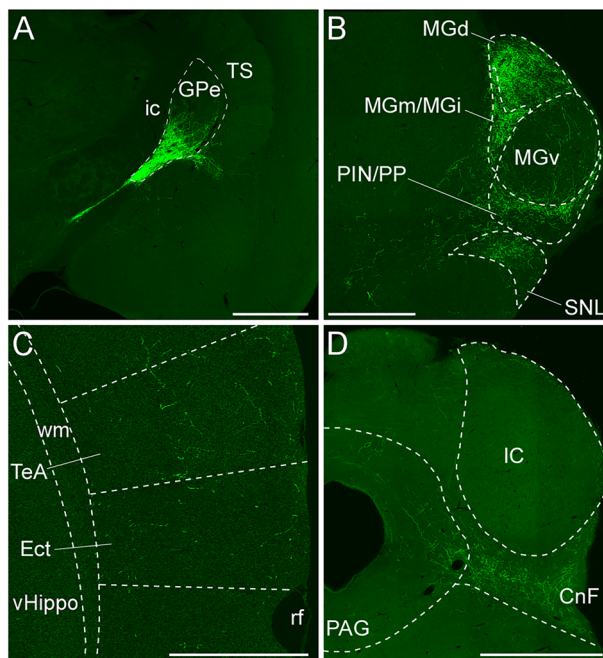


Figure 2. Axonal fibers from GABAergic neurons in the caudal GPe. **A**, AAV2-CAG-FLEX-GFP was injected into the caudal GPe of the GAD67-Cre mouse. GFP-immunoreactive neurons were confined in the caudal GPe. The internal capsule (ic) is shown as a brain region marker. GFP-immunoreactive axonal fibers were distributed in the several subdivisions of MGB and SNL in **B**, in the temporal association cortex (TeA) and Ect in **C**, and CnF and PAG in **D**. Scale bars: 1.0 mm in **A** and **D** and 0.5 mm in **B** and **C**.

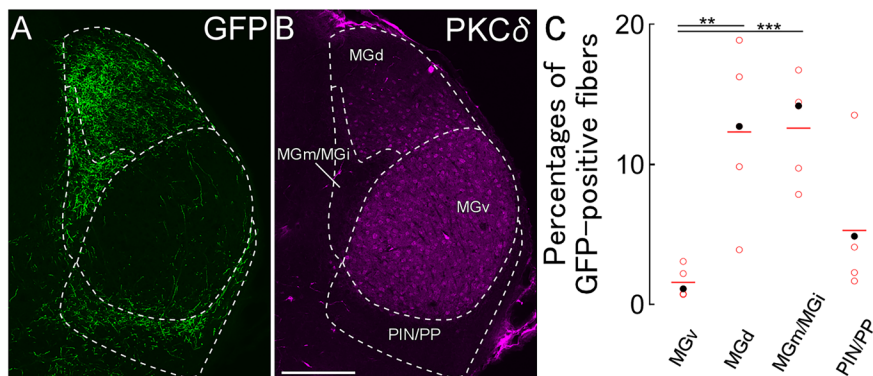


Figure 3. Axonal fibers of GPe GABAergic neurons in the MGB. **A**, **B**, GFP-positive fibers were mainly distributed in MGd, MGm/MGi, and PIN/PP. The boundaries for each subdivision of MGB were defined by PKC δ immunoreactivity. **C**, The densities of GFP-immunoreactive fibers in each subdivision. Each dot indicates the percentage of each mouse. Filled dots are derived from **A**. MGd and MGm/MGi densities were higher than those of MGv (** $p < 0.01$; *** $p < 0.005$). Scale bar, 250 μ m.

Axonal fibers originating from GABAergic neurons in the rostral GPe have previously been observed in the substantia nigra (Kita and Kita, 1994; Bolam et al., 2000; Mallet et al., 2012; Oh et al., 2017). To extend these observations and examine whether GPe GABAergic neurons project to dopaminergic or GABAergic neurons in the substantia nigra, we examined the distribution of GFP-immunoreactive axonal fibers from the caudal GPe using neurochemical markers of the substantia nigra, TH for dopaminergic neurons and PV for GABAergic neurons (Fig. 5; Extended Data Fig. 5-1; 98% of PV-positive neurons are GFP-positive neurons in the SNL of GAD67GFP mice, while none are TH-positive [122 PV-positive neurons in four animals]). The boundary between TH- and PV-immunoreactive regions was distinct in the SNL. Most GFP-immunoreactive fibers were distributed in the TH-immunoreactive region and were in close contact with the TH-immunoreactive somata and dendrites. Only a few GFP-immunoreactive fibers were found in the PV-immunoreactive region. These findings suggest that GABAergic neurons in the caudal GPe may preferentially project to dopaminergic neurons in the SNL, consistent with the projection pattern of the rostral GPe to the substantia nigra par compacta (SNc; Oh et al., 2017).

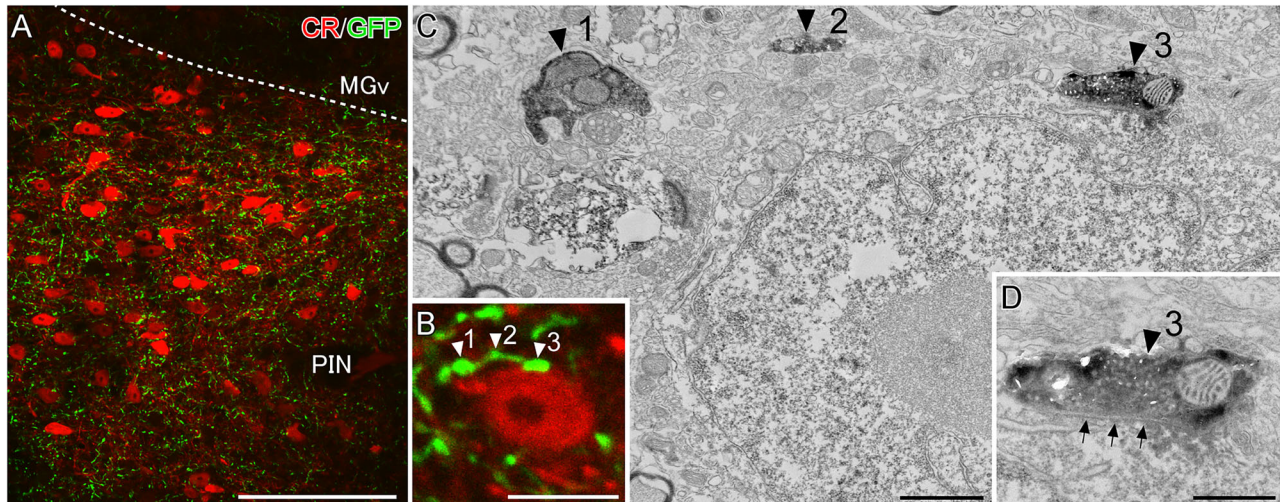


Figure 4. GPe GABAergic fibers forming synaptic contacts on CR-expressing neurons in the PIN. **A**, CR-immunoreactive neurons and numerous GFP-expressing GPe GABAergic fibers are accumulated in the PIN. **B**, Higher-magnification image of a CR-immunoreactive neuron analyzed by CLSM-EM. **C**, An EM image of the same structure shown in **B**. GFP and CR immunoreactivities are visualized using DAB-nickel and DAB, respectively. All three axonal boutons (black arrowheads 1–3) correspond to boutons in **B** (white arrowheads 1–3). **D**, Arrows indicate that a GFP-immunoreactive axon terminal formed a symmetrical synaptic contact on the CR-immunoreactive soma. Scale bars: 100 μm in **A**, 10 μm in **B**, 1 μm in **C**, and 0.5 μm . See Extended Data Figures 4-1 and 4-2 for more details.

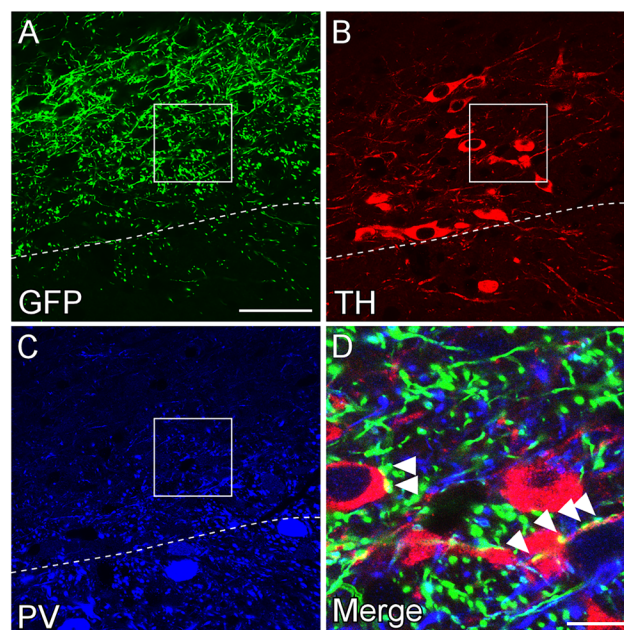


Figure 5. Axonal fibers of GPe GABAergic neurons in the SNL. **A–C**, GFP-positive fibers were mainly distributed in the TH-positive region of SNL. The dashed line indicates the boundary between TH-positive and PV-positive regions. **D**, The enlarged image of the area marked by the rectangle of **A**. GFP-positive fibers form close synaptic apposition with TH-positive soma and dendrites (arrowheads). Scale bars: 50 μm in **A** and 10 μm in **D**. See Extended Data Figure 5-1 for more details.

Neurochemical properties in the caudal GPe

Recent studies have identified several GABAergic subpopulations in the rostral GPe, where distinct subpopulations characterized by neurochemical profiles exhibit specific projection targets (Mallet et al., 2012; Mastro et al., 2014; Abdi et al., 2015; Hernández et al., 2015; Oh et al., 2017; Abecassis et al., 2020). We hypothesized that similar distinct GABAergic subpopulations exist in the caudal GPe and project to specific brain regions. To test this hypothesis, we first examined their heterogeneity in the caudal GPe by using neurochemical markers ChAT, FoxP2, Lhx6, and PV in GAD67-GFP mice. ChAT-immunoreactive neurons were sparsely distributed (7.2% of GPe neurons, $n = 504$ neurons in three animals) and negative for GFP (Fig. 6A,E). In contrast, we observed variations in GFP intensities among GPe

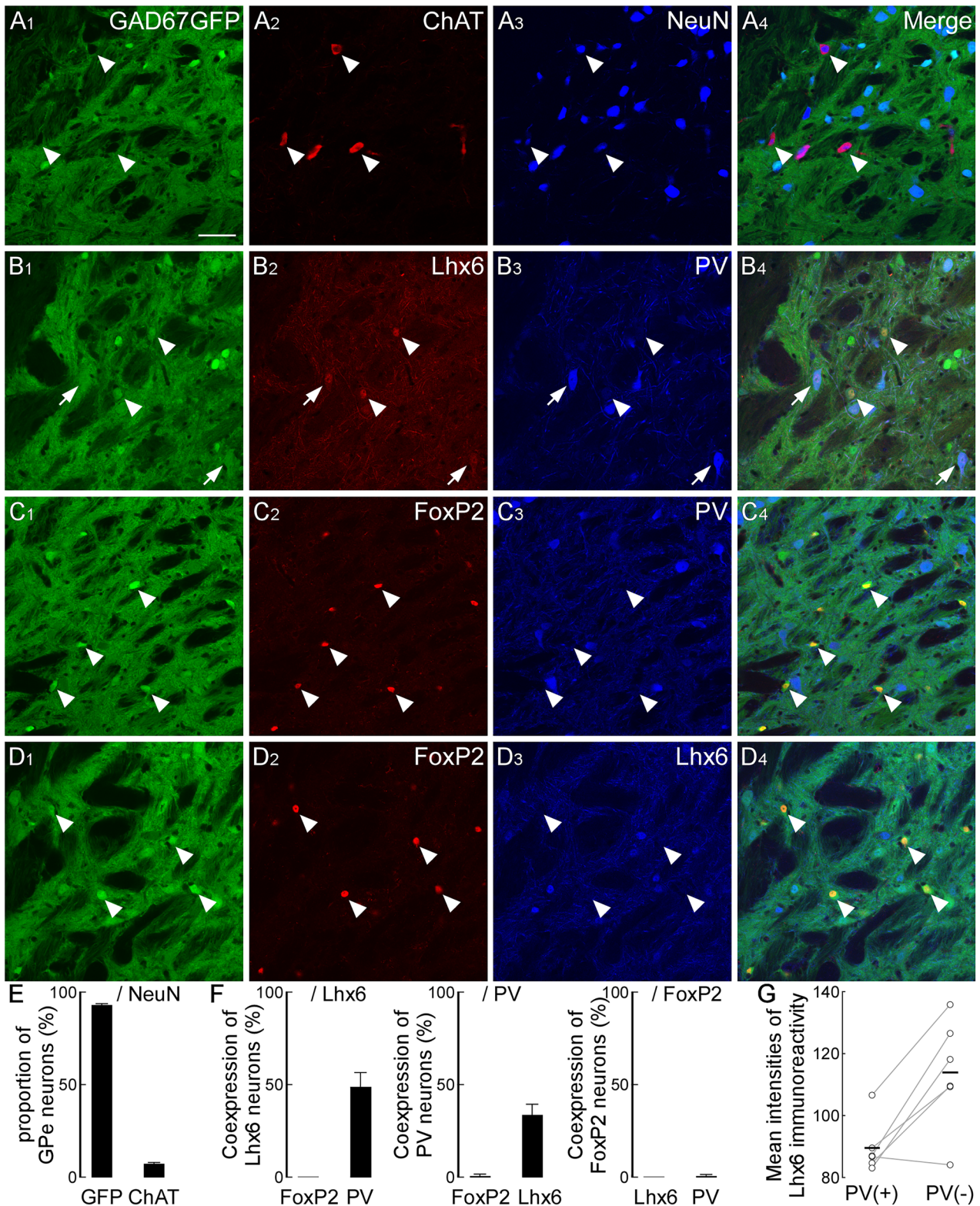


Figure 6. Neurochemical profiles in the caudal GPe. **A**, GABAergic neurons express GFP in the GAD67-GFP mouse. While the somata of neurons strongly expressing GFP could be identified, somata of most GFP-positive neurons were not clearly identified. In contrast, ChAT-positive cholinergic neurons were completely negative for GFP (arrowheads). **B**, Some of Lhx6- and GFP-positive neurons were immunoreactive for PV (arrow), but most of them were negative for PV (arrowheads). **C**, FoxP2-positive neurons exhibited strongly GFP (arrowheads). Almost all of them were negative for PV. **D**, All of FoxP2-positive neurons were negative for Lhx6 (arrowheads). **E**, The vast majority of GPe neurons was GABAergic neurons. **F**, Lhx6-immunoreactive neurons were colocalized with PV immunoreactivity. In contrast, FoxP2-immunoreactive neurons were not colocalized with Lhx6- and PV-immunoreactivities. **G**, Among Lhx6-immunoreactive neurons, PV-positive neurons exhibited significantly weaker Lhx6 immunoreactivity than PV-negative neurons ($*p < 0.05$). Scale bar, 50 μ m.

GABAergic neurons. FoxP2-immunoreactive neurons exhibited relatively strong GFP expression compared with other GPe GABAergic neurons, allowing clear identification of cell bodies (Fig. 6C,D) and consistently negative for Lhx6 (Fig. 6F; all FoxP2+ neurons were negative for Lhx6, $n = 154$ neurons in three animals) or PV (only 1.4% of FoxP2+ neurons were positive for PV, $n = 154$ neurons in three animals). PV-immunoreactive neurons typically displayed relatively large somata, some of which coexpressed Lhx6 [Fig. 6B,F; Lhx6-positive neurons ($n = 107$) and PV-positive neurons ($n = 186$) in four animals]. Among Lhx6-immunoreactive neurons, PV-positive neurons exhibited weaker Lhx6 immunoreactivity than PV-negative neurons (Fig. 6G; $p = 0.0131$; two-tailed paired t test; 37 ± 6 neurons across six animals). Overall, these results indicate that FoxP2-expressing GPe GABAergic neurons constitute a distinct subpopulation. In contrast, Lhx6- or PV-expressing GPe GABAergic neurons would be heterogeneous subpopulations and be further subdivided into three subpopulations: Lhx6-single, PV-single, and Lhx6- and PV-double-expressing. These neurochemical profiles in the caudal GPe are consistent with previous reports in the rostral GPe (Abdi et al., 2015; Hernández et al., 2015; Oh et al., 2017; Abecassis et al., 2020).

The GPe receives GABAergic input from the striatum and glutamatergic input mainly from subcortical regions and rarely from the cortex (Kaneko et al., 2002). Notably, Poisik et al. (2003) have reported the GABAergic subpopulations in the rostral GPe are subdivided by mGluR1-mediated depolarization. We next examined which GPe GABAergic subpopulations express mGluR1a. Immunoreactivity for mGluR1a was observed in the caudal GPe (Fig. 7), as previously reported in the rostral GPe. According to the intensity of mGluR1a immunoreactivity, two distinct subpopulations were observed: one with relatively strong mGluR1a immunoreactivity on the cell membrane, and another with weak mGluR1a expression. The strong mGluR1a-immunoreactive subpopulation was positive for Lhx6 (87.5% of strong mGluR1a+ neurons were positive for Lhx6; $n = 40$ in three animals) but negative for FoxP2 (0% of strong mGluR1a+ neurons were positive for FoxP2; $n = 47$ in three animals) and PV (0% of strong mGluR1a+ neurons were positive for PV; $n = 33$ in three animals). In contrast, the weak mGluR1a-immunoreactive subpopulation was positive for Lhx6 (97.5% of Lhx6+ neurons were positive for weak mGluR1a; $n = 161$ in three animals) and PV (82.6% of PV+ neurons were positive for weak mGluR1a;

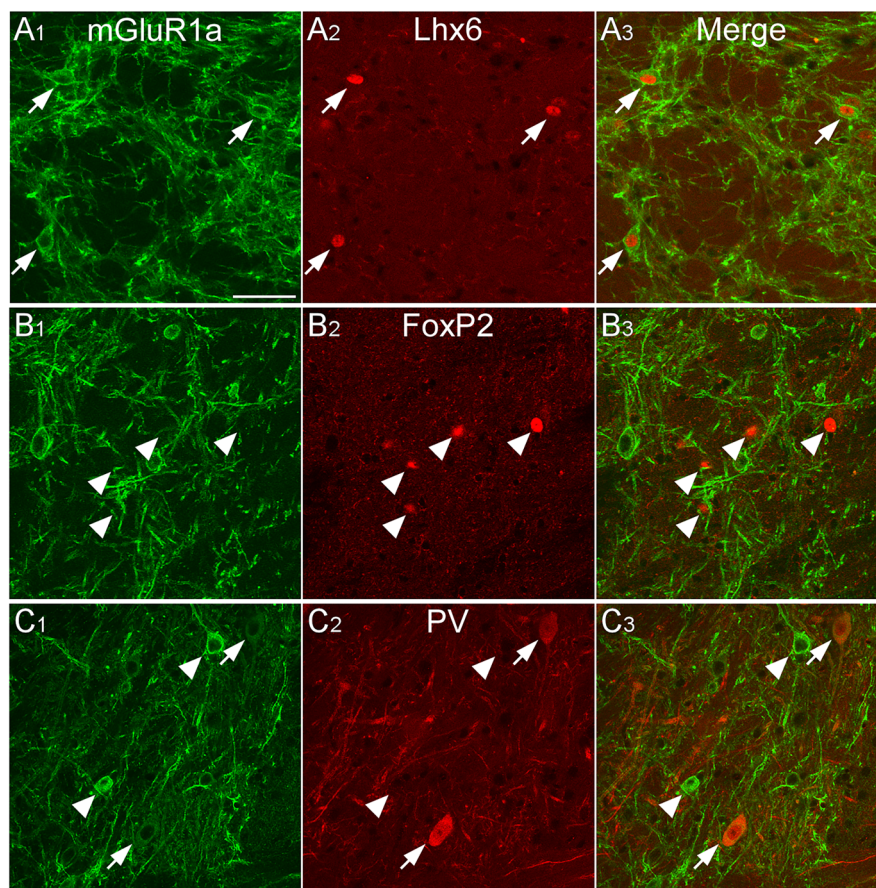


Figure 7. mGluR1a-immunoreactive neurons in the caudal GPe. mGluR1a immunoreactivity was mainly distributed in the dendrites and somata. **A**, Most Lhx6-positive neurons exhibit strong immunoreactivity for mGluR1a (arrowheads). **B**, FoxP2-positive neurons were not immunoreactive for mGluR1a (arrows). **C**, Most PV-positive neurons show weak mGluR1a immunoreactivity (arrowheads). In contrast, strong mGluR1a-immunoreactive neurons were negative for PV immunoreactivity (arrows). Scale bar, 50 μ m.

$n = 172$ in three animals) but negative for FoxP2 (2.5% of FoxP2+ neurons were positive for weak mGluR1a; $n = 197$ in three animals). Overall, some Lhx6-expressing neurons showed strong mGluR1a immunoreactivity, while most Lhx6- or PV-expressing neurons exhibited weak mGluR1a immunoreactivity.

GABAergic projecting neurons in the caudal GPe

We showed that GABAergic neurons in the caudal GPe project to multiple brain regions and examined their heterogeneity using neurochemical profiles. We aimed to identify which subpopulations of GPe neurons project to specific regions. Based on our anterograde experiment (Fig. 2), we focused on three main projection areas: the TeA, MGB, and CnF. The neurochemical profiles of the retrogradely FG-labeled neurons in the caudal GPe were investigated using immunoreactivities for FoxP2, Lhx6, and PV. FG injection into the TeA demonstrated that most retrogradely labeled neurons were positive for Lhx6 in the caudal GPe (Figs. 8, 11; Extended Data Fig. 11-1A; 71.8% of FG- and GFP-double-labeled neurons exhibited Lhx6 immunoreactivity; $n = 39$ in four animals) but not for FoxP2 (5.8% of FG- and GFP-double-labeled neurons exhibited FoxP2 immunoreactivity; $n = 52$ in four animals) or PV (no FG- and GFP-double-labeled neurons exhibited PV immunoreactivity; $n = 39$ in four animals). FG injection into the MGB showed that most retrogradely labeled neurons were positive for PV (Figs. 9, 11; Extended Data Fig. 11-1B; 91.2% of FG- and GFP-double-labeled neurons exhibited PV immunoreactivity; $n = 34$ in four animals) but not for FoxP2 (No FG- and GFP-double-labeled neurons exhibited FoxP2 immunoreactivity; $n = 91$ in four animals) or for Lhx6 (3.7% of FG- and GFP-double-labeled neurons exhibited Lhx6 immunoreactivity; $n = 54$ in four animals). FG injection into the CnF showed that most retrogradely labeled neurons were positive for PV (Figs. 10, 11; Extended Data Fig. 11-1C; 75.4% of FG- and GFP-double-labeled neurons exhibited PV immunoreactivity; $n = 114$ in four animals), followed by Lhx6 (19.6% of FG- and GFP-double-labeled neurons exhibited Lhx6 immunoreactivity; $n = 51$ in four animals), but not for FoxP2 (no FG- and GFP-double-labeled neurons exhibited FoxP2 immunoreactivity; $n = 54$ in four animals). These observations suggest that Lhx6-expressing neurons are a

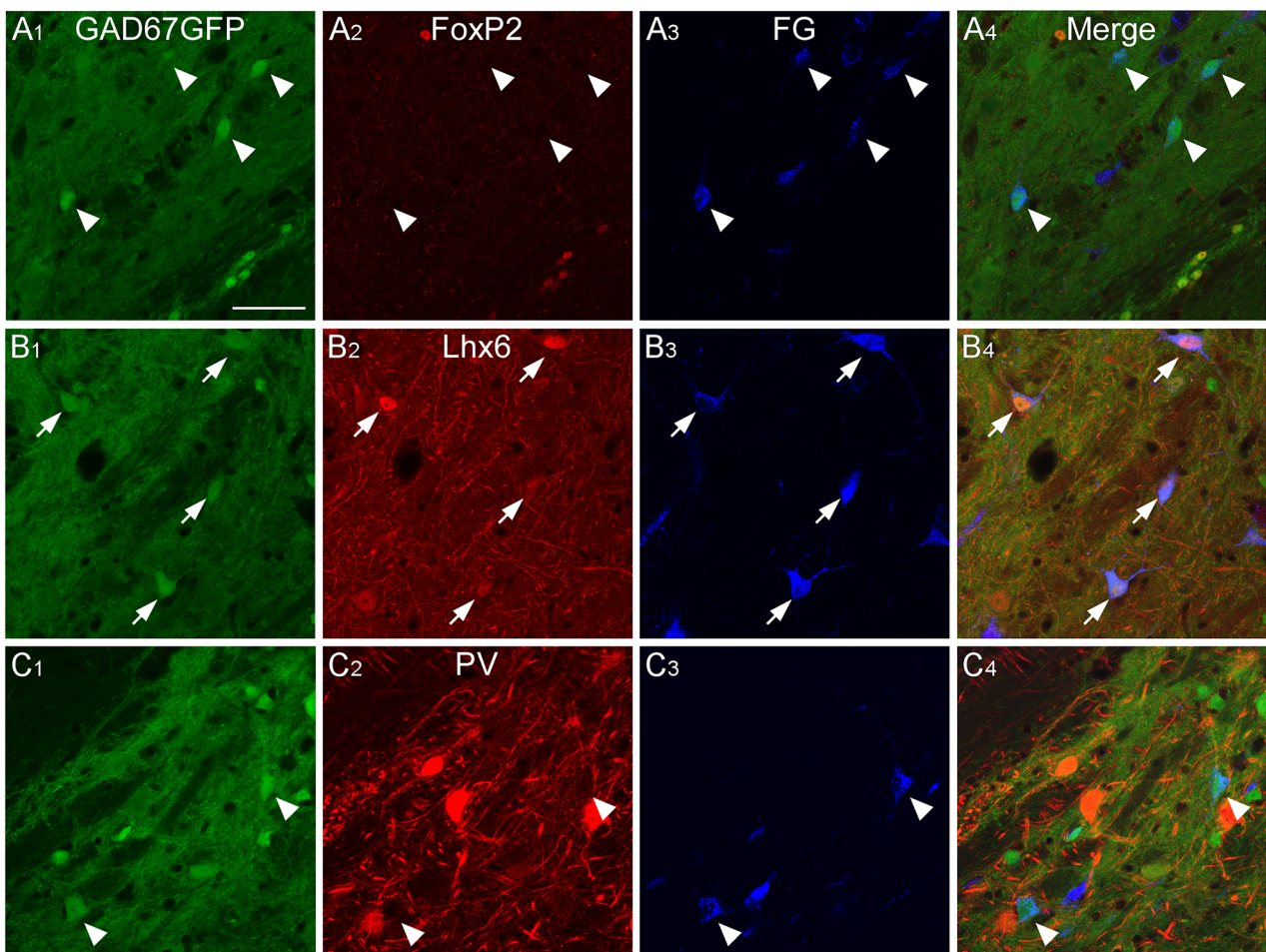


Figure 8. GABAergic neurons projecting to the temporal cortices in the caudal GPe. Injection of the retrograde tracer FG into the TeA of GAD67-GFP mice resulted in FG-labeled neurons in the caudal GPe. FG-labeled GABAergic neurons were positive for Lhx6 immunoreactivity (arrows in **B**), but not for FoxP2 or PV (arrowheads in **A** and **C**). Scale bar, 50 μm .

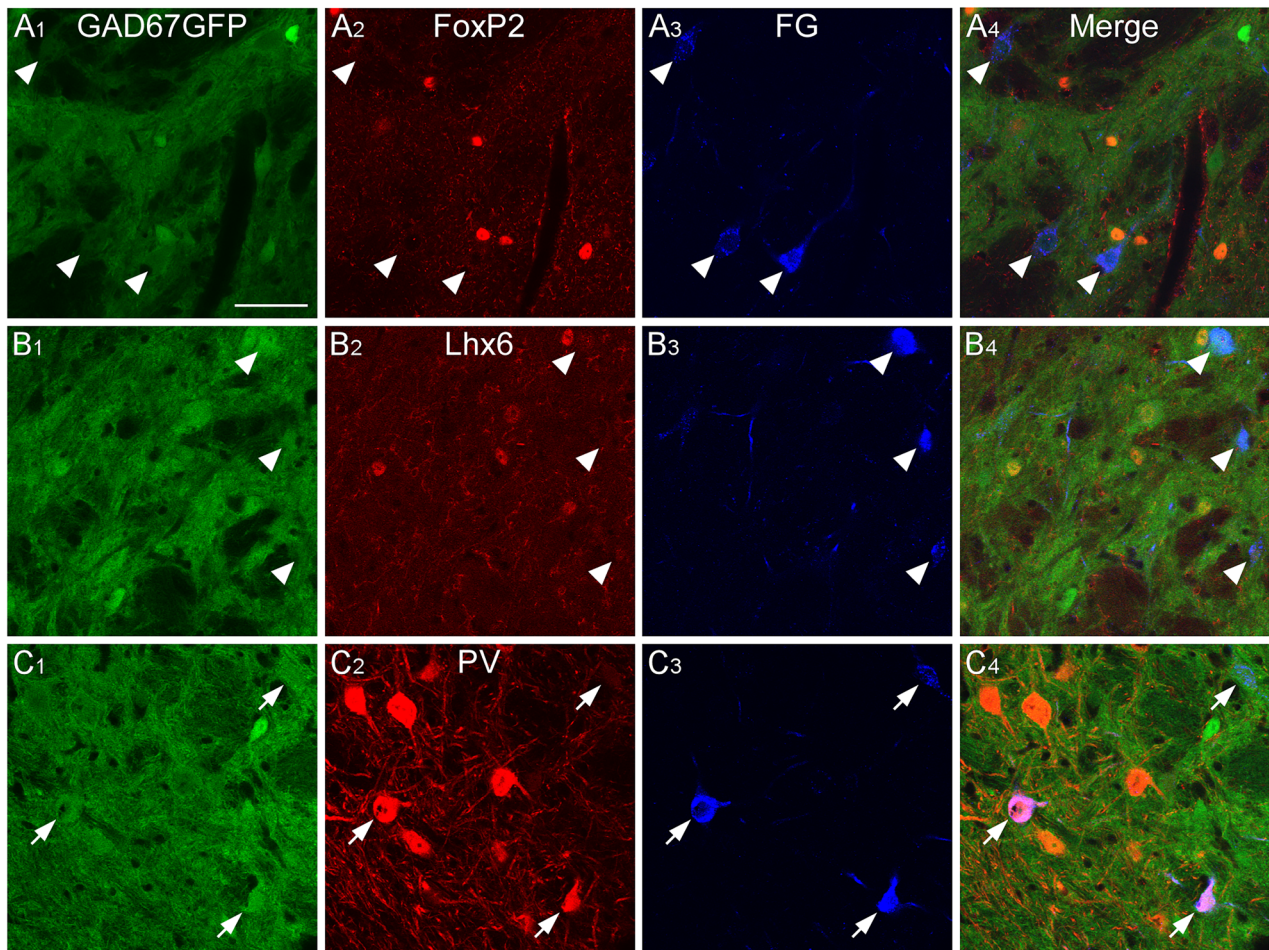


Figure 9. GABAergic neurons projecting to the MGB in the caudal GPe. Injection of FG into the MGB of GAD67-GFP mice resulted in FG-labeled neurons in the caudal GPe. FG-labeled GABAergic neurons were positive for PV immunoreactivity (arrows in **C**), but not for FoxP2 or Lhx6 (arrowheads in **A** and **B**). Scale bar, 50 μm .

distinct subpopulation projecting to the temporal cortices, whereas PV-expressing neurons project to the MGB and CnF. In addition, Lhx6- and PV-expressing neurons may project to the MGB and CnF, although this subpopulation may be minor.

Presynaptic neurons of GABAergic neurons in the caudal GPe

We next investigated presynaptic neurons of GPe GABAergic neurons using the transsynaptic pseudotyped rabies virus expressing mCherry. To express the rabies glycoprotein and avian TVA receptor in GPe GABAergic neurons, we injected the AAV helper virus mixture into the TeA of VGAT-Cre mice (Fig. 12A). Three weeks later, we injected the pseudotyped rabies virus into the caudal GPe. Starter cells, which exhibited both GFP-immunoreactivity and mCherry fluorescence, were localized within the caudal GPe in three mice (Fig. 12B), as illustrated, and further analyzed. Transsynaptically mCherry-labeled presynaptic neurons were predominantly distributed in the TS, secondary in the caudal GPe and neo-cortex including the auditory cortex (Extended Data Fig. 12-1). The mCherry-labeled neurons in the TS were further examined using neurochemical markers to depict the neural circuit of the auditory cortico-basal ganglia loop. Neurons in the direct pathway express PD, whereas those in the indirect pathway express PPE (Le Moine et al., 1990; Lee et al., 1997; Sonomura et al., 2007). Most transsynaptically labeled presynaptic neurons were positive for PD (Fig. 12C; 52.2% of labeled neurons exhibited PD immunoreactivity; $n = 115$ in three animals), and some were positive for PPE (Fig. 12D; 39.2% of labeled neurons exhibited PPE immunoreactivity; $n = 97$ in three animals). Thus, GABAergic neurons in the caudal GPe that project into the TeA receive input from both direct and indirect pathway neurons in the TS. While previous anatomical studies have shown that both direct and indirect pathways project into the rostral GPe (Kawaguchi et al., 1990; Wu et al., 2000; Fujiyama et al., 2011), a recent physiological experiment in the rostral GPe has demonstrated that indirect pathway neurons project into FoxP2-negative prototypic neurons (Ketzel and Silberberg, 2021). This discrepancy may indicate a unique neural circuit in the posterior basal ganglia.

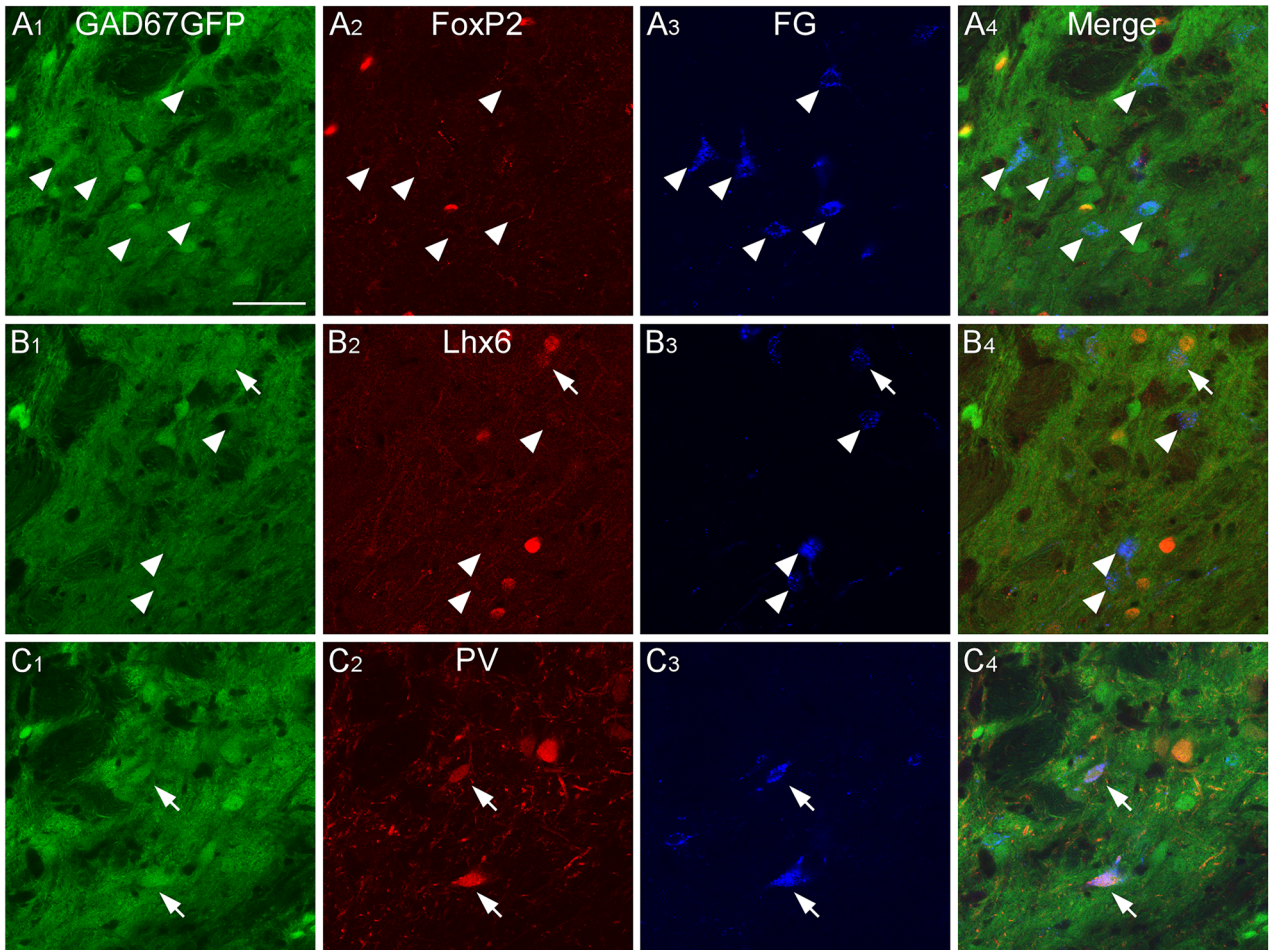


Figure 10. GABAergic neurons projecting to the CnF in the caudal GPe. Injection of FG into the CnF of GAD67-GFP mice resulted in FG-labeled neurons in the caudal GPe. Most FG-labeled GABAergic neurons were positive for PV immunoreactivity (arrows in **C**), but not for FoxP2 or Lhx6 (arrowheads in **A** and **B**). Scale bar, 50 μ m.

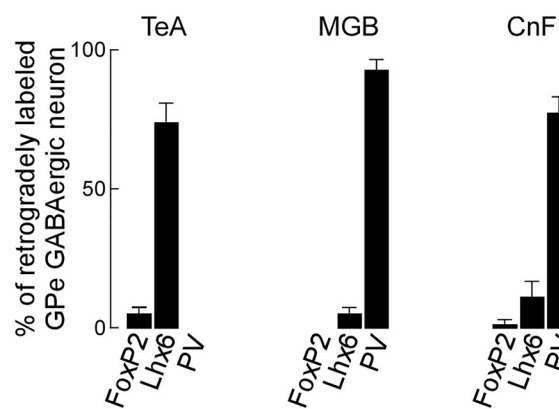


Figure 11. Summary of anatomical and neurochemical profiles in the caudal GPe. Lhx6-expressing neurons in the caudal GPe project into the TeA, whereas PV-expressing neurons into the MGB and CnF. See Extended Data Figure 11-1 for more details.

Because it was reported that unpsuedotyped rabies viruses would be introduced during virus preparation (Watabe-Uchida et al., 2012), we first tested whether the entire system functions in a Cre-dependent manner. AAVretro-CA-FLEX-SADcvsG and AAVretro-EF1a-FLEX-GFP-2A-TVA were injected into A1 of three wild mice, following the injection of pseudotyped rabies virus into the same area (Extended Data Fig. 12-2A). This resulted in no GFP-labeled neuron, a few mCherry-labeled neurons around the injection site (2 ± 2 neurons; mean \pm SD among three mice), and no

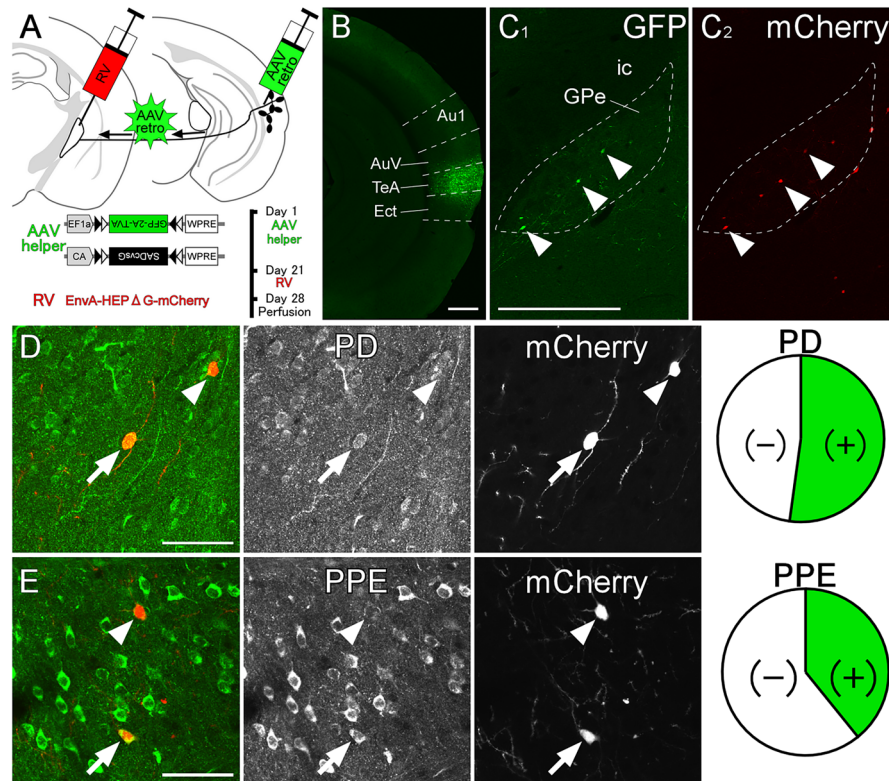


Figure 12. Inputs for GPe GABAergic neurons projecting to the auditory cortex. **A**, The experimental schedule for (1) the injection of AAV helper virus, (2) the pseudotyped rabies virus (RV) injection, and (3) perfusion. **B**, The injection site of AAV helper virus was mainly confined in the TeA. **C**, The starter cells in the caudal GPe were identified by both GFP and mCherry expression (arrowheads). The dashed line indicates the caudal GPe. **D**, **E**, Most of the transsynaptically labeled striatal neurons exhibited PD immunoreactivity (arrow), and some of them exhibited PPE immunoreactivity (arrow). Arrowheads indicate that mCherry-labeled neurons were negative for immunoreactivities. Scale bars, 0.5 mm in **B** and **C**, 50 μ m in **D** and **E**. See Extended Data Figures 12-1 and 12-2 for more details.

mCherry-labeled neurons outside the injection site, indicating this minimal labeling was likely caused by unavoidable contamination with the unspseudotyped rabies virus (Watabe-Uchida et al., 2012). Second, to confirm the distribution of starter cells, AAVretro-EF1a-FLEX-GFP-2A-TVA were injected into the temporal association cortex of VGAT-Cre mice, following the injection of pseudotyped rabies virus into the caudal part of GPe. Immunofluorescence of GFP allowed visualization of even weak GFP signals. Most of mCherry-labeled neurons were distributed in the caudal GPe (Extended Data Fig. 12-2B; 1 ± 1 neurons outside GPe and 18 ± 10 neurons in GPe; mean \pm SD among four mice). GFP-immunoreactive neurons were observed in the caudal GPe, but not in the surrounding areas outside the GPe. Taken together, our method would primarily allow for the labeling of presynaptic neurons of GABAergic neurons in the caudal GPe.

Discussion

The present study contributes to elucidating the auditory cortico-basal ganglia loop in mice (Moriizumi and Hattori, 1992; Shammah-Lagnado et al., 1996; Hintiryan et al., 2016; Hunnicutt et al., 2016; Miyamoto et al., 2018; Cai et al., 2019; Foster et al., 2021; Valjent and Gangarossa, 2021). We first showed that the TS receives auditory input from A1 and projects axonal fibers primarily to the caudal GPe. We further demonstrated that the caudal GPe relays to the temporal cortices via two pathways (Fig. 13). In the primary pathway, PV-expressing GABAergic neurons in the caudal GPe project to the nonlemniscal auditory thalamic nuclei, from where CR-expressing neurons subsequently relay to the temporal cortices (Extended Data Fig. 4-1; Cai et al., 2019; Belén Pardi et al., 2020). In the secondary pathway, Lhx6-expressing GABAergic neurons in the caudal GPe project directly to the temporal cortices. Both pathways of the caudal GPe exert an inhibitory influence on the nonlemniscal auditory pathway. Consequently, the caudal GPe emerged as the principal hub of the auditory cortico-basal ganglia loop. In addition, PV-expressing GABAergic neurons in the caudal GPe project primarily to the CnF and secondarily to dopaminergic neurons in the SNL and PAG. Interestingly, the GPI and SNR, which are considered to be the output nuclei in the basal ganglia, are not involved in the auditory cortico-basal ganglia loop.

Because feedforward projections from the A1 to the temporal cortices predominate over feedback projections (Vaudano et al., 1991; Tasaka et al., 2020), we propose that the auditory cortico-basal ganglia loop function as an open loop (Fig. 13; Joel

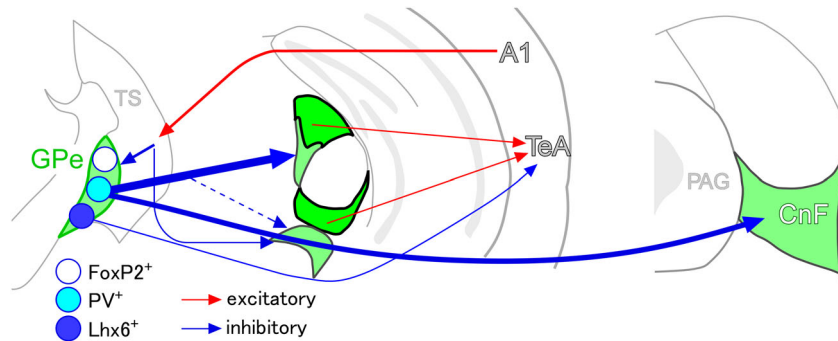


Figure 13. The schematic drawing of the auditory cortico-basal ganglia loop. The A1 sends excitatory efferents into the TS, where direct and indirect pathway neurons project into the caudal GPe. In the caudal GPe, Lhx6-expressing GABAergic neurons directly project to the temporal cortices, including the TeA/Ect/AuV, whereas PV-expressing GABAergic neurons strongly project to the CnF and MGB subdivisions, where CR-expressing neurons send excitatory efferents to the temporal cortices. It is worth noting that both Lhx6-expressing and PV-expressing neurons can directly and indirectly suppress the temporal cortices, respectively.

and Weiner, 1994). Rather than functioning as a closed loop or feedback circuit, the auditory cortico-basal ganglia loop may act as a gate by spontaneously suppressing higher auditory cortices. It is because PV-expressing GABAergic neurons in the GPe, which may exhibit high-frequency spontaneous firing (Ketzel and Silberberg, 2021), could serve as another gate by suppressing the nonlemniscal auditory pathway. Additionally, Lhx6-expressing GABAergic neurons in the GPe could directly suppress the TeA. Thus, when acoustic stimuli activate the auditory cortex, the spontaneous inhibition of GPe GABAergic neurons may be relieved through disinhibition via the auditory cortico-striato-pallida pathway.

Anatomical and neurochemical profiles of GABAergic neurons in the caudal GPe

As previously shown in the rostral GPe, the caudal GPe also consists of a large number of GABAergic neurons and a small number of cholinergic neurons (Fig. 6). Cholinergic neurons in the caudal GPe receive GABAergic input from the TS and project strongly to auditory cortices (Chavez and Zaborszky, 2017). Since the caudal GPe is close to the substantia innominata, cholinergic neurons in the caudal GPe may contribute to acetylcholine-dependent plasticity in the auditory cortex (Guo et al., 2019). From the neurochemical point of view, GPe GABAergic neurons in the caudal GPe can be divided into four major subpopulations. FoxP2-expressing neurons are a distinct subpopulation, as there is little colocalization with other neurochemical markers. Based on the colocalization of other neurochemical markers, we identified three other subpopulations: strong Lhx6-positive and PV-negative neurons; weak Lhx6-positive and PV-positive neurons; and Lhx6-negative and PV-positive neurons. From the anatomical point of view, GABAergic neurons in the caudal GPe can be divided into three major subpopulations. Lhx6-expressing GPe GABAergic neurons mainly projected to the temporal cortices, whereas PV-expressing GPe GABAergic neurons mainly projected to the MGB and CnF. However, in the present study, we were unable to ascertain the target region of FoxP2-expressing neurons, which might project to the striatum as arky pallidal neurons. Overall, our findings align with previous research in the rostral GPe, where distinct subpopulations characterized by neurochemical profiles exhibited specific projection targets (Mallet et al., 2012; Mastro et al., 2014; Abdi et al., 2015; Hernández et al., 2015; Oh et al., 2017; Abecassis et al., 2020). Interestingly, GABAergic neurons in the caudal GPe are likely similar to those in the rostral GPe based on anatomical and neurochemical profiles: PV-expressing neurons in both rostral and caudal GPe project to the thalamus (Mastro et al., 2014), while Lhx6-expressing neurons, which are nearly identical to Nkx2.1- and Npas4-positive neurons (Abecassis et al., 2020), project to the neocortex. It is important to note that the subregions targeted by GABAergic neurons from the rostral GPe differ from those targeted by neurons in the caudal GPe, as the rostral GPe would be integrated into the neural circuitry of distinct systems.

We also distinguished three distinct subpopulations expressing mGluR1a in the caudal GPe: subpopulations that strongly express mGluR1a with Lhx6, those that weakly express mGluR1a with Lhx6 or PV, and those that do not express mGluR1a with FoxP2. Previous electrophysiological studies have indicated that prototypic neurons are influenced by mGluR1a, whereas arky pallidal neurons are not, which aligns with our observations (Poisik et al., 2003). Kaneda et al. (2007) have reported a significant increase in the spontaneous firing rate in vitro with an mGluR1a agonist, suggesting its potential contribution to the sustained higher activity of prototypic neurons. Because the physiological significance of mGluR1a and specific sources of glutamatergic input remain unclear (Kaneko et al., 2002), further investigation is required.

Functional implication of auditory cortico-basal ganglia loop

We demonstrated that the caudal GPe serves as the major output nucleus in the auditory basal ganglia. PV-expressing GPe GABAergic neurons and CR-expressing neurons in nonlemniscal MGB are involved in the cortico-striato-pallido-thalamo-cortical pathway, whereas Lhx6-expressing GPe GABAergic neurons participate in the cortico-striato-pallido-

cortical pathway. Both pathways may suppress neuronal activity in the nonlemniscal auditory pathway. Our anatomical findings suggest that acoustic stimuli can activate neurons in higher auditory cortical areas by disinhibiting via those pathways. Indeed, nonlemniscal MGB and temporal cortices are known to respond to emotional sounds, including pup calls and threatening stimuli (Quirk et al., 1997; Dalmay et al., 2019; Barsy et al., 2020; Belén Pardi et al., 2020; Tasaka et al., 2020; Lee et al., 2021; Luo et al., 2022; Wang et al., 2023). CR-expressing neurons in the PIN/PP, which convey information regarding the association between a conditioned stimulus (neutral tone) and an unconditioned stimulus (footshock) to the lateral amygdala, have been implicated in triggering freezing behavior (Barsy et al., 2020; Belén Pardi et al., 2020). Considering the weak innervation of the central pathway of the auditory system from the caudal GPe, it is plausible that GABAergic neurons in the caudal GPe contribute more to emotional information than to auditory information processing.

We also demonstrated that GABAergic neurons in the caudal GPe directly innervate dopaminergic neurons in the SNL. Interestingly, dopaminergic neurons in the SNL primarily send axonal fibers to the TS (Menegas et al., 2018), suggesting the presence of a striato-pallido-nigral loop. This connection implies that the auditory cortico-basal ganglia loop shares information with dopaminergic neurons in the SNL that project to the TS, encode acoustic stimuli, and reinforce avoidance behavior in response to threatening stimuli and physical salience (Menegas et al., 2018; Akiti et al., 2022). Our anatomical findings suggest that acoustic stimuli can activate dopaminergic neurons in the SNL by disinhibition from the auditory cortico-striato-pallido-nigral pathway. Indeed, acoustic stimuli have been shown to activate dopaminergic neurons in the SNL (Menegas et al., 2018).

In addition, we demonstrated that PV-expressing GABAergic neurons in the caudal GPe project to the CnF. Considering that glutamatergic neurons in the CnF elicit high-speed, synchronous-gait locomotion (Caggiano et al., 2018; Dautan et al., 2021), the auditory GPe→CnF pathway might play an important role in locomotion, including escape-like behaviors (Li et al., 2021). Moreover, this pathway may serve as a substrate for the improvement of walking in patients with Parkinson's disease using rhythmic beats (Nombela et al., 2013).

In summary, the caudal GPe is a principal hub in the auditory cortico-basal ganglia loop. The auditory cortico-basal ganglia loop has an inhibitory effect on the higher auditory thalamic and cortical regions and may be instrumental in defensive behaviors against acoustic stimuli.

References

- Abdi A, et al. (2015) Prototypic and arypallidal neurons in the dopamine-intact external globus pallidus. *J Neurosci* 35:6667–6688.
- Abecassis ZA, et al. (2020) Npas1+Nkx2.1+ neurons are an integral part of the cortico-pallido-cortical loop. *J Neurosci* 40:743–768.
- Akiti K, Tsutsui-Kimura I, Xie Y, Mathis A, Markowitz JE, Anyoha R, Datta SR, Mathis MW, Uchida N, Watabe-Uchida M (2022) Striatal dopamine explains novelty-induced behavioral dynamics and individual variability in threat prediction. *Neuron* 110:3789–3804.
- Alexander GE, DeLong MR, Strick PL (1986) Parallel organization of functionally segregated circuits linking basal ganglia and cortex. *Annu Rev Neurosci* 9:357–381.
- Barsy B, Kocsis K, Magyar A, Babiczky Á, Szabó M, Veres JM, Hillier D, Ulbert I, Yizhar O, Máttyás F (2020) Associative and plastic thalamic signaling to the lateral amygdala controls fear behavior. *Nat Neurosci* 23:625–637.
- Belén Pardi M, Vogenstahl J, Dalmay T, Spanò T, Pu DL, Naumann LB, Kretschmer F, Sprekeler H, Letzkus JJ (2020) A thalamocortical top-down circuit for associative memory. *Science* 370:844–848.
- Bolam JP, Hanley JJ, Booth PAC, Bevan MD (2000) Synaptic organization of the basal ganglia. *J Anat* 196:527–542.
- Caggiano V, Leiras R, Goñi-Errro H, Masini D, Bellardita C, Bouvier J, Caldeira V, Fisione G, Kiehn O (2018) Midbrain circuits that set locomotor speed and gait selection. *Nature* 553:455–460.
- Cai D, et al. (2019) Distinct anatomical connectivity patterns differentiate subdivisions of the nonlemniscal auditory thalamus in mice. *Cereb Cortex* 29:2437–2454.
- Chavez C, Zaborszky L (2017) Basal forebrain cholinergic-auditory cortical network: primary versus nonprimary auditory cortical areas. *Cereb Cortex* 27:2335–2347.
- Dalmay T, et al. (2019) A critical role for neocortical processing of threat memory. *Neuron* 104:1180–1194.
- Dautan D, Kovács A, Bayasgalan T, Diaz-Acevedo MA, Pal B, Mena-Segovia J (2021) Modulation of motor behavior by the mesencephalic locomotor region. *Cell Rep* 36:109594.
- Foster NN, et al. (2021) The mouse cortico-basal ganglia-thalamic network. *Nature* 598:188–194.
- Franklin KBJ, Paxinos G (2007) The mouse brain in stereotaxic coordinates, Ed 3. Cambridge, MA: Academic Press.
- Fujiyama F, Sohn J, Nakano T, Furuta T, Nakamura KC, Matsuda W, Kaneko T (2011) Exclusive and common targets of neostriatofugal projections of rat striosome neurons: a single neuron-tracing study using a viral vector. *Eur J Neurosci* 33:668–677.
- Fukuda T (2017) Structural organization of the dendritic reticulum linked by gap junctions in layer 4 of the visual cortex. *Neuroscience* 340:76–90.
- Gerfen CR, Bolam JP (2016) The neuroanatomical organization of the basal ganglia. In: *Handbook of Behavioral Neuroscience*, 24, pp. 3–32
- Guilhemsang L, Mallet NP (2024) Arypallidal neurons in basal ganglia circuits: unveiling novel pallidostriatal loops? *Curr Opin Neurobiol* 84:102814.
- Guo W, Robert B, Polley DB (2019) The cholinergic basal forebrain links auditory stimuli with delayed reinforcement to support learning. *Neuron* 103:1164–1177.
- Hernández VM, Hegeman DJ, Cui Q, Kolver DA, Fiske MP, Glajch KE, Pitt JE, Huang TY, Justice NJ, Savio Chan C (2015) Parvalbumin + neurons and Npas1 + neurons are distinct neuron classes in the mouse external globus pallidus. *J Neurosci* 35:11830–11847.
- Higo S, Akashi K, Sakimura K, Tamamaki N (2009) Subtypes of GABAergic neurons project axons in the neocortex. *Front Neuroanat* 3:25.
- Hintiryan H, et al. (2016) The mouse cortico-striatal projectome. *Nat Neurosci* 19:1100–1114.
- Hunnicutt BJ, Jongbloets BC, Birdsong WT, Gertz KJ, Zhong H, Mao T (2016) A comprehensive excitatory input map of the striatum reveals novel functional organization. *eLife* 5:e19103.
- Joel D, Weiner I (1994) The organization of the basal ganglia-thalamocortical circuits: open interconnected rather than closed segregated. *Neuroscience* 63:363–379.

- Kaneda K, Kita T, Kita H (2007) Repetitive activation of glutamatergic inputs evokes a long-lasting excitation in rat globus pallidus neurons in vitro. *J Neurophysiol* 97:121–133.
- Kaneko T, Fujiyama F, Hioki H (2002) Immunohistochemical localization of candidates for vesicular glutamate transporters in the rat brain. *J Comp Neurol* 444:39–62.
- Kawaguchi Y, Wilson CJ, Emson PC (1990) Projection subtypes of rat neostriatal matrix cells revealed by intracellular injection of biocytin. *J Neurosci* 10:3421–3438.
- Ketzef M, Silberberg G (2021) Differential synaptic input to external globus pallidus neuronal subpopulations in vivo. *Neuron* 109:516–529.
- Kita H, Kita ST (1994) The morphology of globus pallidus projection neurons in the rat: an intracellular staining study. *Brain Res* 636:308–319.
- Kompoliti K, Metman LV (2010) Encyclopedia of movement disorders.
- Lee T, Kaneko T, Taki K, Mizuno N (1997) Preprodynorphin-, preproenkephalin-, and preprotachykinin-expressing neurons in the rat neostriatum: an analysis by immunocytochemistry and retrograde tracing. *J Comp Neurol* 386:229–244.
- Lee Y, Oh JP, Han JH (2021) Dissociated role of thalamic and cortical input to the lateral amygdala for consolidation of long-term fear memory. *J Neurosci* 34:9561–9570.
- Le Moine C, Normand E, Guitteny AF, Fouque B, Teoule R, Bloch B (1990) Dopamine receptor gene expression by enkephalin neurons in rat forebrain. *Proc Natl Acad Sci U S A* 87:230–234.
- Li Z, Wei JX, Zhang GW, Huang JJ, Zingg B, Wang X, Tao HW, Zhang LI (2021) Corticostriatal control of defense behavior in mice induced by auditory looming cues. *Nat Commun* 12:1040.
- Lim S-J, Fiez JA, Holt LL (2014) How may the basal ganglia contribute to auditory categorization and speech perception? *Front Neurosci* 8:230.
- Llano DA, Sherman SM (2008) Evidence for nonreciprocal organization of the mouse auditory thalamocortical-corticothalamic projection systems. *J Comp Neurol* 507:1209–1227.
- Lu E, Llano DA, Sherman SM (2009) Different distributions of calbindin and calretinin immunostaining across the medial and dorsal divisions of the mouse medial geniculate body. *Hear Res* 257:16–23.
- Luo B, Li J, Liu J, Li F, Gu M, Xiao H, Lei S, Xiao Z (2022) Frequency-dependent plasticity in the temporal association cortex originates from the primary auditory cortex, and is modified by the secondary auditory cortex and the medial geniculate body. *J Neurosci* 42:5254–5267.
- Mallet N, Micklem BR, Henny P, Brown MT, Williams C, Bolam JP, Nakamura KC, Magill PJ (2012) Dichotomous organization of the external globus pallidus. *Neuron* 74:1075–1086.
- Márquez-Legorreta E, Horta-Júnior JdA, Berrebi AS, Saldaña E (2016) Organization of the zone of transition between the pretectum and the thalamus, with emphasis on the pretectothalamic lamina. *Front Neuroanat* 10:82.
- Mastro KJ, Bouchard RS, Holt HAK, Gittis AH (2014) Transgenic mouse lines subdivide external segment of the globus pallidus (GPe) neurons and reveal distinct GPe output pathways. *J Neurosci* 34:2087–2099.
- Menegas W, Akiti K, Amo R, Uchida N, Watabe-Uchida M (2018) Dopamine neurons projecting to the posterior striatum reinforce avoidance of threatening stimuli. *Nat Neurosci* 21:1421–1430.
- Middleton FA, Strick PL (1996) The temporal lobe is a target of output from the basal ganglia. *Proc Natl Acad Sci U S A* 93:8683–8687.
- Miyamoto Y, Katayama S, Shigematsu N, Nishi A, Fukuda T (2018) Striosome-based map of the mouse striatum that is conformable to both cortical afferent topography and uneven distributions of dopamine D1 and D2 receptor-expressing cells. *Brain Struct Funct* 223:4275–4291.
- Mori T, Morimoto K (2014) Rabies virus glycoprotein variants display different patterns in rabies monosynaptic tracing. *Front Neuroanat* 7:47.
- Moriizumi T, Hattori T (1992) Separate neuronal populations of the rat globus pallidus projecting to the subthalamic nucleus, auditory cortex and pedunculo-pontine tegmental area. *Neuroscience* 46:701–710.
- Nombela C, Hughes LE, Owen AM, Grahn JA (2013) Into the groove: can rhythm influence Parkinson's disease? *Neurosci Biobehav Rev* 37:2564–2570.
- Ogata S, Miyamoto Y, Shigematsu N, Esumi S, Fukuda T (2022) The tail of the mouse striatum contains a novel large type of GABAergic neuron incorporated in a unique disinhibitory pathway that relays auditory signals to subcortical nuclei. *J Neurosci* 42:8078–8094.
- Oh SW, et al. (2014) A mesoscale connectome of the mouse brain. *Nature* 508:207–214.
- Oh YM, Karube F, Takahashi S, Kobayashi K, Takada M, Uchigashima M, Watanabe M, Nishizawa K, Kobayashi K, Fujiyama F (2017) Using a novel PV-Cre rat model to characterize pallidonigral cells and their terminations. *Brain Struct Funct* 222:2359–2378.
- Osakada F, Mori T, Cetin AH, Marshel JH, Virgen B, Callaway EM (2011) New rabies virus variants for monitoring and manipulating activity and gene expression in defined neural circuits. *Neuron* 71:617–631.
- Poisk OV, Mannaioni G, Traynelis S, Smith Y, Conn PJ (2003) Distinct functional roles of the metabotropic glutamate receptors 1 and 5 in the rat globus pallidus. *J Neurosci* 23:122–130.
- Ponvert ND, Jaramillo S (2019) Auditory thalamostriatal and corticostriatal pathways convey complementary information about sound features. *J Neurosci* 39:271–280.
- Quirk GJ, Armony JL, LeDoux JE (1997) Fear conditioning enhances different temporal components of tone-evoked spike trains in auditory cortex and lateral amygdala. *Neuron* 19:613–624.
- Saunders A, Oldenburg IA, Berezovskii VK, Johnson CA, Kingery ND, Elliott HL, Xie T, Gerfen CR, Sabatini BL (2015) A direct GABAergic output from the basal ganglia to frontal cortex. *Nature* 521:85–89.
- Seeger CA (2013) The visual corticostriatal loop through the tail of the caudate: circuitry and function. *Front Syst Neurosci* 7:104.
- Shammah-Lagnado SJ, Alheid GF, Heimer L (1996) Efferent connections of the caudal part of the globus pallidus in the rat. *J Comp Neurol* 376:489–507.
- Shigematsu N, Nishi A, Fukuda T (2019) Gap junctions interconnect different subtypes of parvalbumin-positive interneurons in barrels and septa with connectivity unique to each subtype. *Cereb Cortex* 29:1414–1429.
- Simonyan K (2019) Recent advances in understanding the role of the basal ganglia. *F1000Res* 8:122.
- Sitek K, Helou L, Chandrasekaran B (2023) Auditory corticostriatal connections in the human brain. *bioRxiv*.
- Sonomura T, Nakamura K, Furuta T, Hioki H, Nishi A, Yamanaka A, Uemura M, Kaneko T (2007) Expression of D1 but not D2 dopamine receptors in striatal neurons producing neuropeptide B in rats. *Eur J Neurosci* 26:3093–3103.
- Tamamaki N, Yanagawa Y, Tomioka R, Miyazaki JI, Obata K, Kaneko T (2003) Green fluorescent protein expression and colocalization with calretinin, parvalbumin, and somatostatin in the GAD67-GFP knock-in mouse. *J Comp Neurol* 467:60–79.
- Tasaka G-I, Feigin L, Maor I, Groyzman M, DeNardo LA, Schiavo JK, Froemke RC, Luo L, Mizrahi A (2020) The temporal association cortex plays a key role in auditory-driven maternal plasticity. *Neuron* 107:566–579.
- Tomioka R, Sakimura K, Yanagawa Y (2015) Corticofugal GABAergic projection neurons in the mouse frontal cortex. *Front Neuroanat* 9:133.
- Tomioka R, Takemoto M, Song WJ (2023) Neurochemical properties for defining subdivisions of the mouse medial geniculate body. *Hear Res* 431:108724.
- Valjent E, Gangarossa G (2021) The tail of the striatum: from anatomy to connectivity and function. *Trends Neurosci* 44:203–214.
- Vaudano E, Legg CR, Glickstein M (1991) Afferent and efferent connections of temporal association cortex in the rat: a horseradish peroxidase study. *Eur J Neurosci* 3:317–330.
- Wang Y, et al. (2023) A common thalamic hub for general and defensive arousal control. *Neuron* 111:3270–3287.

- Watabe-Uchida M, Zhu L, Ogawa SK, Vamanrao A, Uchida N (2012) Whole-brain mapping of direct inputs to midbrain dopamine neurons. *Neuron* 74:858–873.
- Wu Y, Richard S, Parent A (2000) The organization of the striatal output system: a single-cell juxtacellular labeling study in the rat. *Neurosci Res* 38:49–62.
- Xiong Q, Znamenskiy P, Zador AM (2015) Selective corticostriatal plasticity during acquisition of an auditory discrimination task. *Nature* 521:348–351.
- Zhong R, Qin L, Sato Y (2014) Auditory response properties of neurons in the putamen and globus pallidus of awake cats. *J Neurophysiol* 111:2124–2137.
- Zingg B, Chou XL, Zhang ZG, Mesik L, Liang F, Tao HW, Zhang LI (2017) AAV-mediated anterograde transsynaptic tagging: mapping corticocollicular input-defined neural pathways for defense behaviors. *Neuron* 93:33–47.
- Znamenskiy P, Zador AM (2013) Corticostriatal neurons in auditory cortex drive decisions during auditory discrimination. *Nature* 497:482–485.